

Multiplex Markov Chains

Dane Taylor^{1,*}

¹*Department of Mathematics, University at Buffalo, State University of New York, Buffalo, NY 14260, USA*
(Dated: November 13, 2021)

Multiplex networks are a common modeling framework for interconnected systems and multimodal data, yet we still lack fundamental insights for how multiplexity affects stochastic processes. We introduce a “Markov chains of Markov chains” model such that with probably $(1 - \omega) \in [0, 1]$ random walkers remain in the same layer and follow (layer-specific) *intralayer Markov chains*, whereas with probability ω they move to different layers following (node-specific) *interlayer Markov chains*. By coupling “Markov-chain layers” versus “network layers”, we identify novel multiplexity-induced phenomena including *multiplex imbalance* (whereby the multiplex coupling of reversible Markov chains yields an irreversible one) and *multiplex convection* (whereby a stationary distribution exhibits circulating flows that involve multiple layers). These phenomena (as well as the convergence rate λ_2) are found to exhibit optima for intermediate ω , and we explore their relation to imbalances for the intralayer degrees of nodes. To provide analytical insight, we characterize stationary distributions for when there is timescale separation between transitions within and between layers (i.e., $\omega \rightarrow 0$ and $\omega \rightarrow 1$).

PACS numbers: 89.75.Hc, 02.50.Ga, 87.15.hj, 84.35.+i

Multiplex networks [1]—a type of multilayer network [2, 3] in which layers encode different types of *intralayer* edges, and *interlayer* edges couple the layers—have been used to model interconnection complex systems including transportation networks [4–6], critical infrastructures [7], and different types of relationships [8]. In the context of data science, they provide frameworks for data integration/fusion [9–11] and stratification [12, 13]. Here, we propose a multiplex generalization of Markov chains [14], a memoryless process for stochastic transitions between discrete states, and they provide a theoretical foundation for diverse applications, such as queuing theory [15], population dynamics [16], and machine-learning algorithms that rely on Markov chain Monte Carlo [17], hidden Markov models [18], and/or Markov decision processes [19]. Similar to Markov chains, multiplex Markov chains (MMCs) are expected to find diverse applications within, and beyond, the study of networks.

According to an MMC, random walkers move along (layer-specific) *intralayer Markov chains* with probability $\omega \in [0, 1]$, and with probability $1 - \omega$ they transition to new layers following (node-specific) *interlayer Markov chains*. MMCs can be used to study random walks on multiplex networks, and diffusion physics for multiplex networks is already a burgeoning field [20–26]. Most approaches rely on a generalization of the graph Laplacian called a supraLaplacian matrix, which can be constructed by first multiplexing the network layers’ adjacency matrices into a supra-adjacency matrix, and then creating a Laplacian matrix by treating the supra-adjacency matrix as if it were a normal adjacency matrix (i.e., neglecting that intra- and interlayer edges are different). Both normalized [20] and unnormalized supraLaplacians [21–26] have been studied, and in the latter case, one can simply couple the unnormalized Laplacians of layers. Other formulations have also been proposed to study centrality and consensus [27–32]. Despite the significant advances that have been made, this field remains in its infancy [33].

By coupling “Markov-chain layers” rather than “network

layers,” we identify and study novel multiplexity-induced phenomena including *multiplex imbalance* and *multiplex convection*, which—along with the convergence rate λ_2 —are found to be optimized at intermediate ω . These properties are shown to have an interesting and complicated relation to the imbalances of nodes’ intralayer degrees. We analyze MMCs with spectral perturbation theory to characterize the stationary distribution when there is a separation of timescales between intra- and interlayer transitions: As $\omega \rightarrow 0$, intralayer Markov chains each approach (local) stationary solutions, and these (layer-specific) solutions are balanced by the interlayer Markov chains. Analogously, as $\omega \rightarrow 1$ the interlayer Markov chains individually approach (local) stationary solutions, and these (node-specific) solutions are balanced by the intralayer Markov chains. This work also reveals that the optimality for $\lambda_2(\omega)$ is an inherent property of MMCs.

Model. Consider a set of *intralayer Markov chains* (the “layers”) with size- N transition matrices $\mathbf{P}^{(i)}$ for $i \in \{1, \dots, I\}$ and a set of (node-specific) *interlayer Markov chains* with size- I transition matrices $\tilde{\mathbf{P}}^{(n)}$ for $n \in \{1, \dots, N\}$. Each $P_{nm}^{(i)}$ scales the transition probability from node n to m in layer i , while $\tilde{P}_{ij}^{(n)}$ scales the transition probability from layer i to j for node n . Or equivalently, these give transitions between node-layer pairs: from (n, i) to (m, i) in the case of $P_{nm}^{(i)}$, and from (n, i) to (n, j) in the case of $\tilde{P}_{ij}^{(n)}$.

A (discrete-time) multiplex Markov chain (MMC) is a stochastic process in which the states are node-layer pairs (n_p, i_p) , which we enumerate $p \in \{1, \dots, NI\}$, yielding $n_p = (p \bmod N)$ and $i_p = \lceil p/N \rceil$ (‘mod’ and $\lceil \cdot \rceil$ indicate the modulus and ceiling functions, respectively.) Transitions between states follow a *supratransition matrix*

$$\mathbb{P}(\omega) = (1 - \omega)\text{diag}\left(\{\mathbf{P}^{(i)}\}\right) + \omega \sum_n \tilde{\mathbf{P}}^{(n)} \otimes \mathbf{E}^{(n)}. \quad (1)$$

Coupling strength $\omega \in [0, 1]$ tunes the probability that random walks use interlayer vs intralayer Markov chains, $\text{diag}(\cdot)$

is a block-diagonal matrix in which the argument matrices are placed along the diagonal, \otimes denotes the Kronecker product, and $\mathbf{E}^{(n)} = \mathbf{e}^{(n)}[\mathbf{e}^{(n)}]^T$, where $\mathbf{e}_m^{(n)} = 1$ if $n = m$ and 0 otherwise. Each $[\mathbb{P}(\omega)]_{pq}$ gives the transition probability from (n_p, i_p) to (n_q, i_q) . Under the assumption of *uniform coupling*, we let $\tilde{\mathbf{P}}^{(n)} = \tilde{\mathbf{P}} \forall n$, and the last term in Eq. (1) simplifies to $\omega \tilde{\mathbf{P}} \otimes \mathbf{I}$, where \mathbf{I} is a size- N identity matrix.

We define a (continuous-time) MMC with a normalized supraLaplacian $\mathbb{L}(\omega) = \mathbb{I} - \mathbb{P}(\omega)$. \mathbb{I} is a size- (NI) identity matrix, and $[\mathbb{L}(\omega)]_{pq}$ are rates for transitions between node-layer pairs. We will focus on discrete-time MMCs due to the wealth of existing knowledge on supraLaplacians [20–26].

Let $\mathbf{x}^{(t)}$ be a length- NI row vector such that $[\mathbf{x}^{(t)}]_p$ gives the expected fraction of random walkers at node-layer pair (n_p, i_p) at time t . Given initial condition $\mathbf{x}^{(0)}$, $\mathbf{x}^{(t)}$ evolves following a linear discrete map $\mathbf{x}^{(t+1)} = \mathbf{x}^{(t)}\mathbb{P}(\omega)$. If $\mathbb{P}(\omega)$ is nonnegative, irreducible, and aperiodic, then $\mathbf{x}^{(t)} \rightarrow \mathbf{v}(\omega)$ converges to a unique stationary distribution, which is the left dominant eigenvector of $\mathbb{P}(\omega)$. It is convenient to define $\pi_{n_p}^{(i_p)}(\omega) = [\mathbf{v}(\omega)]_p$ and to drop the subscript p , so that $\pi_n^{(i)}(\omega)$ is the density of walkers at node n in layer i .

Application to a multiplex network. MMCs provide a new form of diffusion on multiplex networks. Let $\mathbf{P}^{(i)} = [\mathbf{D}^{(i)}]^{-1}\mathbf{A}^{(i)}$ and $\tilde{\mathbf{P}}^{(n)} = [\tilde{\mathbf{D}}^{(n)}]^{-1}\tilde{\mathbf{A}}^{(n)}$ denote intra- and interlayer transition matrices, respectively, of Markov chains derived from a multiplex network in which $\mathbf{A}^{(i)}$ and $\tilde{\mathbf{A}}^{(n)}$ are intra- and interlayer adjacency matrices, and $\mathbf{D}^{(i)}$ and $\tilde{\mathbf{D}}^{(n)}$ are diagonal matrices with entries $\mathbf{D}_{nn}^{(i)} = \sum_m A_{nm}^{(i)}$ and $\tilde{\mathbf{D}}_{ii} = \sum_j \tilde{A}_{ij}^{(n)}$ that encode the intra- and interlayer node degrees. In Fig. 1(A), we visualize such an MMC in which $\mathbf{P}^{(1)}$ and $\mathbf{P}^{(2)}$ are intralayer transition matrices associated with chain and star networks (both are undirected and unweighted). Self-edges are added to the first and last nodes of the chain to make it 2-regular. We enumerate the nodes $n \in \{1, \dots, 11\}$ clockwise around the chain, starting at the center node. We implement uniform coupling with $\tilde{\mathbf{P}} = \begin{bmatrix} 0 & 1 \\ 1 & 0 \end{bmatrix}$. Node colors in Fig. 1(A) depict $\pi_n^{(i)}(\omega)$ for $\omega = 0.5$. Note that $\pi_n^{(i)}(\omega)$ is largest for node-layer pair $(n, i) = (1, 2)$ (the hub node in the star network); $\pi_n^{(i)}(\omega)$ is also large for node-layer pair $(1, 1)$, since it is coupled to $(1, 2)$ by an interlayer edge.

Observe for layer $i = 1$ that the $\pi_n^{(i)}(\omega)$ values monotonically decrease as one moves clockwise around the chain. That is, the $\pi_n^{(i)}(\omega)$ values of MMCs are influenced by the global structure, which can be beneficial, for example, if one seeks to study the importances of nodes and/or layers [29, 31, 32]. This contrasts diffusions based on unnormalized supraLaplacians [21–26] (since their stationary distribution is the uniform distribution) and the normalized supraLaplacian of [20] (whose entries are proportional to the node-layer pairs' *total degrees*). See the Supplementary Material for further discussion.

Multiplex imbalance and convection. The $\pi_n^{(i)}(\omega)$ values reflect a complicated interplay between intra- and interlayer Markov chains, which we further study through the stationary flows $\mathbb{F}_{pq}(\omega) = \pi_{n_p}^{(i_p)}(\omega)[\mathbb{P}(\omega)]_{pq}$ across edges. We de-

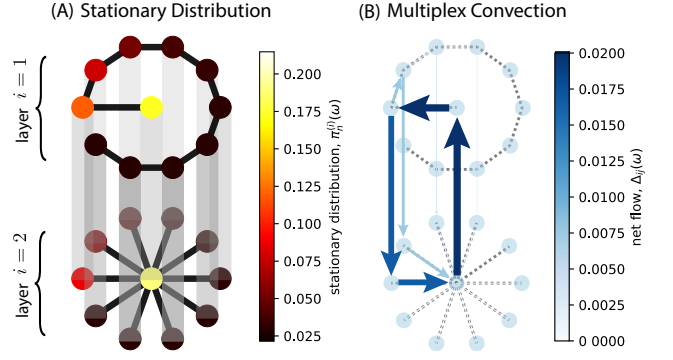


FIG. 1. **Multiplex imbalance and convection.** (A) Stationary distribution $\pi_n^{(i)}(\omega)$ for a discrete-time multiplex Markov chain (MMC) with interlayer coupling strength $\omega = 0.5$. The solid black and opaque grey lines indicate edges in the intra- and interlayer Markov chains, respectively. (B) Stationary net flow $\Delta_{pq}(\omega) = \pi_{n_p}^{(i_p)}(\omega)[\mathbb{P}(\omega)]_{pq} - \pi_{n_q}^{(i_q)}(\omega)[\mathbb{P}(\omega)]_{qp}$. Observe the emergence of a cycle, which we call *multiplex convection*. This arises here due to *multiplex imbalance*: an emergent phenomenon where the multiplexing of reversible Markov chains yields an irreversible MMC.

compose $\mathbb{F}(\omega)$ into its symmetric, $(\mathbb{F}_{pq} + \mathbb{F}_{qp})/2$, and skew symmetric, $\Delta_{pq}/2$, components to define the *stationary flow imbalance* $\Delta_{pq} = \mathbb{F}_{pq} - \mathbb{F}_{qp}$ across each edge. $\Delta_{pq} > 0$ indicates that there is a greater flow from (n_p, i_p) and (n_q, i_q) , whereas $\Delta_{pq} < 0$ indicates the opposite. We quantify the *total flow imbalance* $\|\Delta\|_F$ using the Frobenius norm, and a Markov chain is *reversible* iff $\|\Delta\|_F = 0$ (i.e., $\Delta_{pq} = 0 \forall p, q$). We define *multiplex imbalance* as the phenomenon whereby the multiplex coupling of reversible Markov chains yields an irreversible MMC. In that case, $\|\Delta\|_F$ quantifies the total multiplex imbalance.

In Fig. 1(B), we visualize Δ_{pq} for the MMC from Fig. 1(A). Observe that these values exhibit a circulating flow imbalance involving more than one layer, which we call *multiplex convection*. Because $\mathbf{P}^{(1)}$, $\mathbf{P}^{(2)}$ and $\tilde{\mathbf{P}}$ are all transition matrices of reversible Markov chains, the irreversibility of the MMC is an emergent multiplexity-induced property. It is worth noting that multiplex convection does not require multiplex imbalance, nor vice versa, and so these are related, but notably different, phenomena.

Timescale separations. We now analyze $\pi_n^{(i)}(\omega)$ for two limits: Walkers rarely move between layers as $\omega \rightarrow 0$, which yields a type of layer decoupling. Walkers rarely remain in the same layer as $\omega \rightarrow 1$, which yields a type of layer aggregation.

Given intra- and interlayer Markov chains with transition matrices $\mathbf{P}^{(i)}$ and $\tilde{\mathbf{P}}^{(n)}$, respectively, let $\mathbf{v}^{(i)}$ and $\tilde{\mathbf{v}}^{(n)}$ denote their stationary distributions. Note that they are left eigenvectors associated with an eigenvalue equal to 1. Let $\tilde{\mathbf{e}}^{(i)}$ be a length- I unit vector (i.e., $\tilde{e}_j^{(i)} = 1$ if $j = i$ and 0 otherwise). Setting $\omega = 0$ in Eq. (1) yields $\mathbb{P}(0) = \text{diag}(\{\mathbf{P}^{(i)}\})$, for which $\lambda_1 = 1$ is an eigenvalue with an I -dimensional left eigenspace spanned by vectors $\mathbf{v}^{(i)} = \tilde{\mathbf{e}}^{(i)} \otimes \mathbf{v}^{(i)}$. However, for any positive ω (even an infinitesimally small $\omega > 0$),

Perron-Frobenius theory for nonnegative matrices [34] ensures that the eigenvalue $\lambda_1 = 1$ of $\mathbb{P}(\omega)$ has a 1-dimensional eigenspace spanned by a unique left dominant eigenvector $\mathbb{v}(\omega)$. Moreover, the continuity of eigenvector subspaces [35] requires $\mathbb{v}(\omega)$ to converge within the subspace $\text{span}(\mathbb{v}^{(i)})$, implying there exist constants $\tilde{\alpha}_i$ such that $\lim_{\omega \rightarrow 0} \mathbb{v}(\omega) = \sum_i \tilde{\alpha}_i \mathbb{v}^{(i)}$. We denote $\tilde{\alpha} = [\tilde{\alpha}_1, \dots, \tilde{\alpha}_T]$.

In the Supplementary Material, we show that $\tilde{\alpha}$ is the dominant left eigenvector of an “effective” interlayer transition matrix $\tilde{\mathbf{X}}$ with entries $\tilde{X}_{ij} = \sum_n v_n^{(i)} \tilde{P}_{ij}^{(n)}$. Using the notation $[\mathbb{v}(\omega)]_p = \pi_n^{(i_p)}(\omega)$, we have

$$\lim_{\omega \rightarrow 0} \pi_n^{(i)}(\omega) = \tilde{\alpha}_i v_n^{(i)}. \quad (2)$$

That is, each intralayer Markov chain i obtains its stationary distribution $\mathbf{v}^{(i)}$, and these local solutions are balanced by the stationary distribution of an “effective” interlayer Markov chain that depends on all inter- and intralayer Markov chains. In the case of uniform coupling, $\tilde{\mathbf{P}}^{(n)} = \tilde{\mathbf{P}}$, $\tilde{\mathbf{X}} = \tilde{\mathbf{P}}$, and $\tilde{\alpha} = \tilde{\mathbf{v}}$ (the left dominant eigenvector of $\tilde{\mathbf{P}}$).

We analyze the limit $\omega \rightarrow 1$ in a similar way, except we first implement a change of basis via the (unitary) stride-permutation matrix \mathbb{U} that reorders the node-layer pairs as layer-node pairs: $[\mathbb{U}]_{pq} = 1$ if $q = \lceil p/N \rceil + T[(p-1) \bmod N]$ and $[\mathbb{U}]_{pq} = 0$ otherwise. Matrix $\mathbb{Q}(\omega) = \mathbb{U}\mathbb{P}(\omega)\mathbb{U}^T$ is a suprtransition matrix for the same MMC as $\mathbb{P}(\omega)$; the only difference is that the rows and columns have been permuted. We obtain $\mathbb{Q}(\omega) = (1-\omega) \sum_i \mathbf{P}^{(i)} \otimes \tilde{\mathbf{E}}^{(i)} + \omega \text{diag}(\{\tilde{\mathbf{P}}^{(n)}\})$, where $\tilde{\mathbf{E}}^{(i)} = \tilde{\mathbf{e}}^{(i)}[\tilde{\mathbf{e}}^{(i)}]^T$ and $\tilde{\mathbf{e}}^{(i)}$ is a length- I unit vector. Observe that the form of $\mathbb{Q}(\omega)$ qualitatively matches that of Eq. (1); only the inter- and intralayer transition matrices have been swapped. Thus, one can equally interpret an MMC as intralayer Markov chains coupled by intralayer ones, or as interlayer Markov chains coupled by intralayer ones. These are formally the same. We can thus make use of our earlier results to obtain

$$\lim_{\omega \rightarrow 1} \pi_n^{(i)}(\omega) = \alpha_n \tilde{v}_i^{(n)}, \quad (3)$$

where $\alpha = [\alpha_1, \dots, \alpha_N]$ is the dominant left eigenvector of a transition matrix \mathbf{X} with entries $X_{nm} = \sum_i \tilde{v}_i^{(n)} P_{nm}^{(i)}$ for an “effective” intralayer Markov chain.

In Fig. 2, we validate the accuracy of Eqs. (2) and (3) for the MMC shown in Fig. 1. The observed $\pi_n^{(i)}(\omega)$ values for small and large ω were computed with $\omega = 10^{-3}$ and $\omega = 1 - 10^{-3}$.

Optimal imbalance and convergence rate. Next, we show that total multiplex imbalance $\|\Delta\|_F$ is maximized at some value $\omega_{\Delta}^* = \text{argmax}_{\omega} \|\Delta\|_F \in (0, 1)$. We use the same interlayer Markov chains as in Fig. 1, but now allow the interlayer Markov chains to be different for every node: $\tilde{\mathbf{P}}^{(n)} = \begin{bmatrix} 1-a_n & a_n \\ a_n & 1-a_n \end{bmatrix}$, where $a_n \in [a, 1]$ tunes the probability of switching layers at each node n . We consider four strategies for choosing a_n : (I) $a_n = a$ for each n ; (II) $a_n = a + (n-1)\delta a$ for $n \in \{1, \dots, N\}$ with $\delta a = (1-a)/(N-1)$;

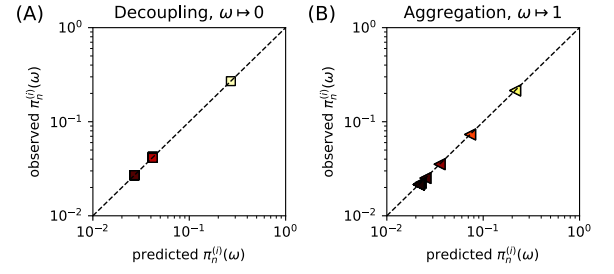


FIG. 2. **Validation of theory for timescale separations.** We compare observed and predicted values of $\pi_n^{(i)}(\omega)$ for the MMC from Fig. 1 for two limiting cases: (A) Eq. (2) for $\omega \rightarrow 0$; and (B) Eq. (3) for $\omega \rightarrow 1$. The symbols’ colors correspond to the same color scale as that shown in Fig. 1(A). Note that 22 symbols are plotted in each panel, but because they overlap, we perceive just a few.

(III) $a_n = 1 - (n-1)\delta a$; and (IV) a_n is sampled uniformly at random from $[a, 1]$.

In Fig. 3(A), we plot $\|\Delta\|_F$ versus ω ; each panel depicts a different strategy. First, because $a \rightarrow 1$ recovers the interlayer transition matrix used in Fig. 1 for all strategies, the (blue solid) curves for $a = 0.99$ are nearly identical in all panels. As a decreases, the different strategies yield different $\|\Delta\|_F$ curves: (I)–(II) the curves for identical and increasing a_n flatten as a decreases and the location of the optimum shifts toward larger ω ; (III) the $\|\Delta\|_F$ curves for decreasing a_n are insensitive to a ; and (IV) the curves for random a_n seem to change randomly, but generally decrease. These responses can be understood by noting that a_1 strongly varies with a for the first two strategies, it remains unchanged for the decreasing- a_n strategy, and it is random for the last strategy, although its expectation decreases. Parameter a_1 determines the optimality of $\|\Delta\|_F$ in this case, because the net flow Δ_{pq} is largest from node-layer pair $(1, 2)$ to $(1, 1)$ [see Fig. 1(B)],

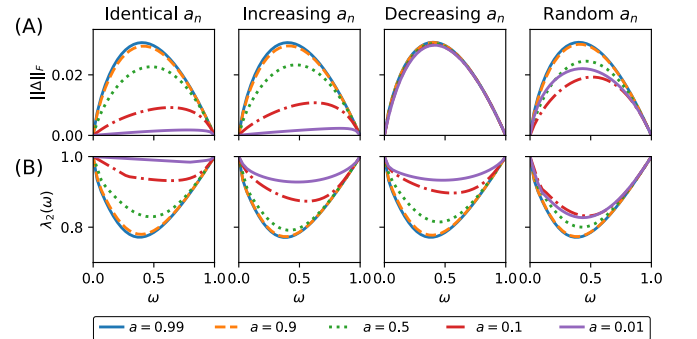


FIG. 3. **Optimal imbalance and convergence rate.** (A) Total multiplex imbalance $\|\Delta\|_F$ and (B) convergence rate $\lambda_2(\omega)$ versus ω for the same intralayer Markov chains as in Fig. 1, but with node-specific interlayer Markov chains in which a_n tunes the probability of switching layers at node n . We choose $a_n \in [a, 1]$ via four strategies: (left) $a_n = a \forall n$; (center left) evenly spaced and monotonically increasing with n ; (center right) evenly spaced and monotonically decreasing with n ; (far right) sampled uniformly at random. We define $\omega_{\Delta}^* = \text{argmax}_{\omega} \|\Delta\|_F$ and $\omega_{\lambda_2}^* = \text{argmax}_{\omega} \lambda_2(\omega)$.

and a_1 tunes the probability of walkers make this transition.

In Fig. 3(B), we show that $\lambda_2(\omega)$ —the second-largest-in-magnitude eigenvalue of $\mathbb{P}(\omega)$ —is also optimized at similar values of ω . Because $\mathbb{x}_p^{(t)} \rightarrow \pi_{n_p}^{(i_p)}(\omega)$ with $t \rightarrow \infty$ as $\mathcal{O}(\lambda_2^t(\omega))$, $\lambda_2(\omega) \in (0, 1)$ is called the *convergence rate*. Importantly, because we found $\mathbb{P}(\omega)$ to have I -dimensional and N -dimensional dominant eigenspaces when $\omega = 0$ and $\omega = 1$, respectively, and due to the continuity of eigenvalues [35], it follows that $\lambda_2(\omega) \rightarrow 1$ in either limit. Furthermore, $d\lambda_2(\omega)/d\omega < 1$ at $\omega = 0$ and $d\lambda_2(\omega)/d\omega > 1$ at $\omega = 1$, and so Rolle’s theorem [36] guarantees that a minimum exists.

Interestingly, the locations ω_Δ^* and $\omega_{\lambda_2}^*$ of optima for $\|\Delta\|_F$ and $\lambda_2(\omega)$ appear to be strongly correlated for some strategies. We explore this further in Supplementary Material, but generally find that there does not seem to be a simple relationship between multiplex imbalance, convection and the optimality of $\|\Delta\|_F$ and $\lambda_2(\omega)$.

Application to brain networks reveals mechanism for multiplex imbalance. Next, we study a mechanism that contributes to the optimality of multiplex imbalance: Δ_{pq} is often large for an interlayer edge associated with a node n such that its intralayer degrees $d_n^{(i_p)}$ and $d_n^{(i_q)}$ are imbalanced (where $d_n^{(i)} = \sum_m A_{nm}^{(i)}$). Observe in Fig. 1(B), for example, that Δ_{pq} is largest from node-layer pair (1, 2) to (1, 1), and this edge is also associated with the largest imbalance of intralayer degrees: $d_1^{(2)} = 10$, $d_1^{(1)} = 2$, and $d_1^{(2)} - d_1^{(1)} = 8$ (recall the chain layer has self-edges to make it 2-regular). We now further study this phenomenon for a MMC representation of an (empirical) multiplex brain network [12] with $N = 148$ nodes (brain regions) and $I = 7$ layers, which represent pairwise coherences of magnetoencephalography (MEG) signals at different frequency ranges: $\{[1, 4], [4, 8], [8, 10.5], [10.5, 13], [13, 20], [20, 30], [30, 45]\}$, which are measured in Hz. We uniformly couple the layers with an interlayer Markov chain with transition matrix: $\tilde{P}_{ij} = 1$ if $|i - j| = 1$ and $i \in \{1, 7\}$, $\tilde{P}_{ij} = 1/2$ if $|i - j| = 1$ and $i \notin \{1, 7\}$, and $\tilde{P}_{ij} = 0$ otherwise.

In Fig. 4, we plot Δ_{pq} versus $(d_{n_p}^{(i_p)} - d_{n_q}^{(j_q)})$ separately for (A) intralayer edges (i.e., $i_p = i_q$) and (B) interlayer edges (i.e., $n_p = n_q$). (Since $\Delta_{pq} = -\Delta_{qp}$, we only plot the positive curves.) Different columns show results for different ω . First, observe that Δ_{pq} are approximately $50\times$ larger for interlayer edges than for intralayer edges [i.e., compare the y-axis of (B) to that of (A)]. Also, note that Δ_{pq} obtain their largest magnitudes near $\omega = 0.5$ (center column), which is consistent with our finding that $\omega_\Delta^* \approx 0.5$ for this MMC. The strong correlation between Δ_{pq} and $(d_{n_p}^{(i_p)} - d_{n_q}^{(j_q)})$ supports out hypothesis that the largest Δ_{pq} occur for interlayer edges associated with the largest intralayer-degree imbalance, $(d_{n_p}^{(i_p)} - d_{n_q}^{(j_q)})$. In Supplementary Material, we study the Pearson correlation coefficient R between Δ_{pq} and $(d_n^{(i)} - d_n^{(j)})$ for frequency-multiplexed brain networks of 50 persons: 25 healthy and 25 with Alzheimer’s disease. For healthy persons and $\omega = 0.5$, we find $R = 0.52$ (-0.37) for interlayer (intralayer) edges.

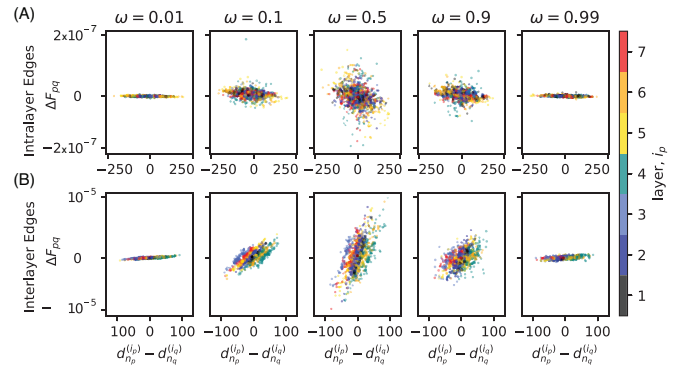


FIG. 4. **Multiplex imbalance and degree imbalance for a frequency-multiplexed functional brain network.** We separately plot Δ_{pq} versus $(d_{n_p}^{(i_p)} - d_{n_q}^{(j_q)})$ for (A) intralayer edges and (B) interlayer edges for a MMC representation of an empirical brain network with $N = 148$ nodes (brain regions) and $I = 7$ layers (correlated MEG signals at different frequency ranges). Δ_{pq} and $(d_{n_p}^{(i_p)} - d_{n_q}^{(j_q)})$ are positively (negatively) correlated for interlayer (intralayer) edges, and Δ_{pq} have their largest magnitudes for $\omega = 0.5$ (center column).

For persons with Alzheimer’s disease, we find $R = 0.56$ (-0.37). We also find $\max_\omega \|\Delta\|_F$ to be 6.6% larger, on average, for persons with Alzheimer’s disease. Given our observation that imbalanced intralayer degrees contribute to multiplex imbalance and convection, and both are increased for persons with Alzheimer’s disease, our findings are consistent with previous work that found persons with Alzheimer’s disease to have a loss of brain inter-frequency hubs [12].

Conclusion. We formulated MMCs as the multiplexing of intra- and interlayer Markov chains, explored novel physical phenomena, and developed a theoretical foundation using perturbation theory. Our work was inspired by the study of diffusion on multiplex networks [20–32], and we focused our attention on aspects of MMCs that are in striking contrast to these models. In particular, stationary distributions of MMCs can yield multiplex imbalance and convection. These emergent, multiplex-induced phenomena, along with the convergence rate λ_2 , were shown to be optimized for intermediate coupling of Markov chains. These new insights for how multiplexity affects stochastic processes provide a step forward in bringing multiplexity theory to Markov-chain applications within, and beyond, the study of networks [15–19].

DT thanks Per Sebastian Skardal and Naoki Masuda for helpful feedback on this manuscript. DT was supported in part by the Simons Foundation (grant #578333).

* danet@buffalo.edu

- [1] E. Cozzo, G. F. De Arruda, F. A. Rodrigues, and Y. Moreno, *Multiplex Networks: Basic Formalism and Structural Properties* (Springer, 2018).
- [2] S. Boccaletti, G. Bianconi, R. Criado, C. Del Genio, J. Gómez-Gardeñes, M. Romance, I. Sendina-Nadal, Z. Wang, and

- M. Zanin, *Physics Reports* **544**, 1 (2014).
- [3] M. Kivelä, A. Arenas, M. Barthelemy, J. P. Gleeson, Y. Moreno, and M. A. Porter, *Journal of Complex Networks* **2**, 203 (2014).
- [4] D. Taylor, F. Klimm, H. A. Harrington, M. Kramár, K. Mischaikow, M. A. Porter, and P. J. Mucha, *Nature Communications* **6**, 7723 (2015).
- [5] E. Strano, S. Shai, S. Dobson, and M. Barthelemy, *Journal of The Royal Society Interface* **12**, 20150651 (2015).
- [6] A. Solé-Ribalta, A. Arenas, and S. Gómez, *New Journal of Physics* **21**, 035003 (2019).
- [7] Y. Y. Haimes and P. Jiang, *Journal of Infrastructure Systems* **7**, 1 (2001).
- [8] D. Krackhardt, *Social Networks* **9**, 109 (1987).
- [9] M. De Domenico, V. Nicosia, A. Arenas, and V. Latora, *Nature Communications* **6**, 1 (2015).
- [10] D. Taylor, S. Shai, N. Stanley, and P. J. Mucha, *Physical Review Letters* **116**, 228301 (2016).
- [11] D. Taylor, R. S. Caceres, and P. J. Mucha, *Physical Review X* **7**, 031056 (2017).
- [12] J. Guillon, Y. Attal, O. Colliot, V. La Corte, B. Dubois, D. Schwartz, M. Chavez, and F. D. V. Fallani, *Scientific Reports* **7**, 1 (2017).
- [13] D. Soriano-Paños, L. Lotero, A. Arenas, and J. Gómez-Gardeñes, *Physical Review X* **8**, 031039 (2018).
- [14] J. G. Kemeny and J. L. Snell, *Markov Chains* (Springer-Verlag, New York, 1976).
- [15] D. G. Kendall, *The Annals of Mathematical Statistics* **24**, 338 (1953).
- [16] J. Kingman, *Journal of Applied Probability* **6**, 1 (1969).
- [17] W. R. Gilks, S. Richardson, and D. Spiegelhalter, *Markov Chain Monte Carlo in Practice* (Chapman and Hall/CRC, 1995).
- [18] L. Tierney, *The Annals of Statistics*, 1701 (1994).
- [19] R. Parr and S. J. Russell, in *Advances in Neural Information Processing Systems* (1998) pp. 1043–1049.
- [20] P. J. Mucha, T. Richardson, K. Macon, M. A. Porter, and J.-P. Onnela, *Science* **328**, 876 (2010).
- [21] S. Gómez, A. Díaz-Guilera, J. Gómez-Gardeñes, C. J. Pérez-Vicente, Y. Moreno, and A. Arenas, *Physical Review Letters* **110**, 028701 (2013).
- [22] A. Solé-Ribalta, M. De Domenico, N. E. Kouvaris, A. Diaz-Guilera, S. Gomez, and A. Arenas, *Physical Review E* **88**, 032807 (2013).
- [23] F. Radicchi and A. Arenas, *Nature Physics* **9**, 717 (2013).
- [24] M. De Domenico, A. Solé-Ribalta, S. Gómez, and A. Arenas, *Proceedings of the National Academy of Sciences* **111**, 8351 (2014).
- [25] A. Tejedor, A. Longjas, E. Foufoula-Georgiou, T. T. Georgiou, and Y. Moreno, *Physical Review X* **8**, 031071 (2018).
- [26] G. Cencetti and F. Battiston, *New Journal of Physics* **21**, 035006 (2019).
- [27] I. Trpevski, A. Stanoev, A. Koseska, and L. Kocarev, *New Journal of Physics* **16**, 113063 (2014).
- [28] M. De Domenico, A. Solé-Ribalta, E. Omodei, S. Gómez, and A. Arenas, *Nature Communications* **6**, 6868 (2015).
- [29] D. Taylor, S. A. Myers, A. Clauset, M. A. Porter, and P. J. Mucha, *Multiscale Modeling & Simulation* **15**, 537 (2017).
- [30] D. R. DeFord and S. D. Pauls, *Journal of Complex Networks* **6**, 353 (2018).
- [31] D. Taylor, M. A. Porter, and P. J. Mucha, “Supracentrality analysis of temporal networks with directed interlayer coupling,” in *Temporal Network Theory*, edited by P. Holme and J. Saramäki (Springer International Publishing, 2019) pp. 325–344.
- [32] D. Taylor, M. A. Porter, and P. J. Mucha, arXiv preprint arXiv:1904.02059 (2019).
- [33] M. De Domenico, C. Granell, M. A. Porter, and A. Arenas, *Nature Physics* **12**, 901 (2016).
- [34] R. B.apat and T. E. S. Raghavan, *Nonnegative Matrices and Applications*, Vol. 64 (Cambridge University Press, Cambridge, UK, 1997).
- [35] T. Kato, *Perturbation Theory for Linear Operators*, Vol. 132 (Springer Science & Business Media, 2013).
- [36] P. Sahoo and T. Riedel, *Mean Value Theorems and Functional Equations* (World Scientific, 1998).

Supplementary Material for “Multiplex Markov Chains”

Dane Taylor^{1,*}

¹Department of Mathematics, University at Buffalo, State University of New York, Buffalo, NY 14260, USA

(Dated: November 13, 2021)

I. COMPARISON OF MMCS TO AN EXISTING MODEL FOR DIFFUSION ON MULTIPLEX NETWORKS

The diffusion model that most closely resembles MMCs is the one proposed in [1], which introduces a suprtransition matrix

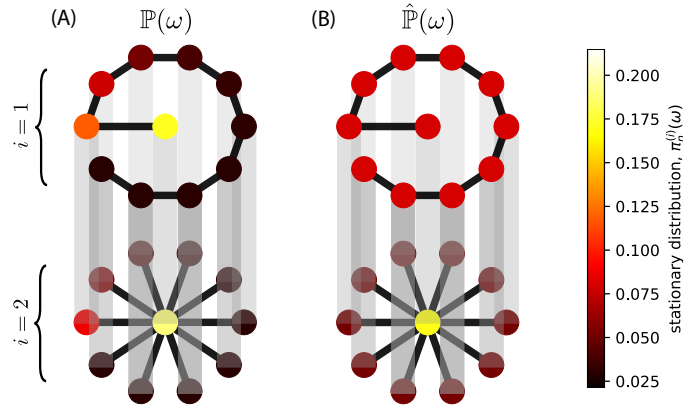
$$\hat{\mathbb{P}}(\omega) = \mathbb{D}(\omega)^{-1} \mathbb{A}(\omega), \quad (1)$$

where $\mathbb{A}(\omega) = (1 - \omega) \text{diag}(\mathbf{A}^{(1)}, \dots, \mathbf{A}^{(I)}) + \omega \tilde{\mathbf{A}} \otimes \mathbf{I}$ is a *supra-adjacency matrix*, and $\mathbb{D}(\omega)$ is a diagonal matrix that encodes the nodes’ total degrees: $[\mathbb{D}(\omega)]_{pp} = \sum_q [\mathbb{A}(\omega)]_{pq} = (1 - \omega) d_{n_p}^{(i_p)} + \omega \tilde{d}_i^{(n_p)}$. Eq. (1) is actually slightly different from the one defined in [1], but theirs is spectrally equivalent and can be recovered by dividing $\mathbb{A}(\omega)$ by $(1 - \omega)$, so that their coupling strength is equivalent to $\omega/(1 - \omega) \in [0, \infty)$. We use the definition of Eq. (1) since it allows us to study the same range of ω as for MMcs, $\omega \in [0, 1]$. Also, it’s worth noting that [1] studied a continuous-time random walk with the goal of extending Markov stability [2], whereas here we study a discrete-time random walk.

In Supplementary Fig. 1, we compare the stationary distribution $\pi_n^{(i)}(\omega)$ for (A) the example MMC from the main text to (B) the stationary distribution $\hat{\pi}_n^{(i)}(\omega)$ associated with $\hat{\mathbb{P}}(\omega)$. Because $\mathbb{A}(\omega)$ is an adjacency matrix for an undirected network, $\hat{\mathbb{P}}(\omega)$ has a stationary distribution with entries that are proportional to the degrees [3]—or in this case, the node-layer pairs:

$$\hat{\pi}_n^{(i)}(\omega) \propto (1 - \omega) d_n^{(i)} + \omega \tilde{d}_i. \quad (2)$$

That is, the $\hat{\pi}_n^{(i)}(\omega)$ values are not informative of a multiplex networks’ global (i.e., nonlocal) properties.



Supplementary Figure 1. **Comparison of an MMC to a model for diffusion on a multiplex network.** We plot the stationary distribution $\pi_n^{(i)}(\omega)$ for (A) the example MMC from the main text and (B) an existing model for diffusion that is based on the suprtransition matrix $\hat{\mathbb{P}}(\omega)$ given by Eq. (1) that does not distinguish between intra- and interlayer edges. Because the multiplex network is undirected, the stationary distribution associated with $\hat{\mathbb{P}}(\omega)$ is not informative of global structure, but only reflects the nodes’ total degrees: $\pi_n^{(i)}(\omega) \propto (1 - \omega) d_n^{(i)} + \omega \tilde{d}_i^{(n)}$.

It’s worth noting that Mucha et. al. [1] do not study a discrete-time random walk, but instead they use $\hat{\mathbb{P}}(\omega)$ to define a normalized supraLaplacian $\hat{\mathbb{L}}(\omega) = \mathbb{I} - \hat{\mathbb{P}}(\omega)$ and study $\frac{d}{dt} \mathbf{x}(t) = -\hat{\mathbb{L}}(\omega)^T \mathbf{x}(t)$. This, however, has the same stationary distribution as $\hat{\mathbb{P}}(\omega)$. One could also formulate a consensus algorithm following $\frac{d}{dt} \mathbf{x}(t) = -\hat{\mathbb{L}}(\omega) \mathbf{x}(t)$, in which case the stationary distribution is the uniform distribution, $\pi_n^{(i)}(\omega) = 1/(NI)$ for every (n, i) . The stationary distribution of a diffusion process following an unnormalized supraLaplacian, $\mathbb{L}(\omega) = \mathbb{D}(\omega) - \mathbb{A}(\omega)$ [4–9], is also also uniform distributions.

* danet@buffalo.edu

II. SPECTRAL PERTURBATION THEORY FOR TIMESCALE SEPARATION

We first study the dominant eigenvector of a supratransition matrix $\mathbb{P}(\omega)$ in the limit $\omega \rightarrow 0^+$, which corresponds to when transitions rarely occur using an interlayer Markov chain.

Let $\mu_1^{(i)}$, $\mathbf{v}^{(i)}$, and $\mathbf{u}^{(i)}$ denote the largest positive eigenvalue and corresponding left and right eigenvectors of each transition matrix $\mathbf{P}^{(i)}$ of the intralayer Markov chains, where $i \in \{1, \dots, I\}$ is a layer index. Furthermore, let $\tilde{\mu}_1^{(n)}$, $\tilde{\mathbf{v}}^{(n)}$, and $\tilde{\mathbf{u}}^{(n)}$ denote the same mathematical elements for each transition matrix $\tilde{\mathbf{P}}^{(n)}$ of the interlayer Markov chains, where $n \in \{1, \dots, N\}$ is a node index. Note that $\mu_1^{(i)} = \tilde{\mu}_1^{(n)} = 1$ for any i and n , since the transition matrices are row stochastic. Also, their corresponding right eigenvectors $\mathbf{u}^{(i)} = [1, \dots, 1]^T$ and $\tilde{\mathbf{u}}^{(n)} = [1, \dots, 1]^T$ are vectors in which all the entries are ones. It is advantageous to let the left eigenvectors represent probability distributions, and so we normalize them in 1-norm. We do not normalize the right eigenvectors (i.e., $\sum_n u_n^{(i)} = N$ and $\sum_i \tilde{u}_i^{(n)} = I$) so that $[\mathbf{v}^{(i)}]^T \mathbf{u}^{(i)} = \sum_n v_n^{(i)} = 1$ and $[\tilde{\mathbf{v}}^{(n)}]^T \tilde{\mathbf{u}}^{(n)} = \sum_i \tilde{v}_i^{(n)} = 1$ for any i and n . Provided that the transition matrices $\mathbf{P}^{(i)}$ and $\tilde{\mathbf{P}}^{(n)}$ are nonnegative and irreducible, Perron-Frobenius theory for nonnegative matrices [10] guarantees that the left eigenvectors $\mathbf{v}^{(i)}$ and $\tilde{\mathbf{v}}^{(n)}$ are unique and contain positive entries.

Turning our attention to the spectra of $\mathbb{P}(\omega)$, we denote its largest positive eigenvalue by $\lambda_1(\omega)$ and its left and right eigenvectors by $\mathbf{v}(\omega)$ and $\mathbf{u}(\omega)$, respectively. We can write the dominant eigenvector equations as

$$\begin{aligned} \mathbb{P}(\omega)^T \mathbf{v}(\omega) &= \mathbf{v}(\omega) \\ \mathbb{P}(\omega) \mathbf{u}(\omega) &= \mathbf{u}(\omega). \end{aligned} \quad (3)$$

Because $\mathbb{P}(\omega)$ is row stochastic for any $\omega \in [0, 1]$, $\mathbf{u}(\omega) = \mathbf{u} = [1, \dots, 1]^T$ is a right eigenvector with eigenvalue $\lambda_1(\omega) = \lambda_1 = 1$. That is, both are independent of ω , and we can drop ω as an argument. (This will be more rigorously supported in a theorem below.)

Provided that $\mathbb{P}(\omega)$ is a nonnegative irreducible matrix, $\mathbf{v}(\omega)$ and $\mathbf{u}(\omega)$ are uniquely defined and have positive entries [10]. Note that this explicitly assumes $\omega \in (0, 1)$. We denote the $\omega \rightarrow 0^+$ limits of $\mathbf{v}(\omega)$ and $\mathbf{u}(\omega)$ by $\mathbf{u}(0^+)$. However, when $\omega = 0$ (i.e., ω is exactly zero), then $\mathbb{P}(\omega)$ is not irreducible. We provide the following theorem to characterize the eigenspace associated with $\lambda_1 = 1$ in this case.

Theorem II.1 *Let $\mathbb{P}(\omega)$ be a supracentrality matrix of a multiplex Markov chain and assume that each intralayer transition matrix $\mathbf{P}^{(i)}$ is nonnegative, irreducible. Then the geometric and algebraic multiplicity of eigenvalue $\lambda_1 = 1$ of $\mathbb{P}(0)$ are both I (recall that I is the number of intralayer Markov chains), and the left and right eigenspaces are spanned by orthogonal eigenvectors*

$$\begin{aligned} \mathbf{v}^{(i)} &= \mathbf{e}^{(i)} \otimes \mathbf{v}^{(i)} \\ \mathbf{u}^{(i)} &= \mathbf{e}^{(i)} \otimes \mathbf{u}^{(i)}, \end{aligned} \quad (4)$$

respectively, where $\mathbf{e}^{(i)}$ denotes the unit vector (i.e., all entries are zero except for the i -th entry, which is a 1) and \otimes denotes the Kronecker product.

Remark II.2 *We refer to the vectors $\mathbf{v}^{(i)}$ and $\mathbf{u}^{(i)}$ as ‘block vectors’, and they consist of zeros, except in the i -th blocks, which are $\mathbf{v}^{(i)}$ and $\mathbf{u}^{(i)}$, respectively.*

Proof. *First, we show that $\mathbf{v}^{(i)}$ and $\mathbf{u}^{(i)}$ are left and right eigenvectors of $\mathbb{P}(0)$ corresponding to the eigenvalue $\lambda_1 = 1$,*

$$\begin{aligned} \mathbb{P}(0) \mathbf{u}^{(i)} &= \mathbf{e}^{(i)} \otimes \mathbf{P}^{(i)} \mathbf{u}^{(i)} \\ &= \mathbf{e}^{(i)} \otimes \mu_1^{(i)} \mathbf{u}^{(i)} \\ &= \mathbf{u}^{(i)} \end{aligned} \quad (5)$$

and

$$\begin{aligned} \mathbb{P}(0)^T \mathbf{v}^{(i)} &= \mathbf{e}^{(i)} \otimes [\mathbf{P}^{(i)}]^T \mathbf{v}^{(i)} \\ &= \mathbf{e}^{(i)} \otimes \mu_1^{(i)} \mathbf{v}^{(i)} \\ &= \mathbf{v}^{(i)}. \end{aligned} \quad (6)$$

It is also straightforward to show that these sets of eigenvectors are orthogonal:

$$\begin{aligned}
[\mathbf{v}^{(i)}]^T \mathbf{v}^{(j)} &= (\mathbf{e}^{(i)} \otimes \mathbf{v}^{(i)})^T (\mathbf{e}^{(j)} \otimes \mathbf{v}^{(j)}) \\
&= ([\mathbf{e}^{(i)}]^T \otimes [\mathbf{v}^{(i)}]^T) (\mathbf{e}^{(j)} \otimes \mathbf{v}^{(j)}) \\
&= [\mathbf{e}^{(i)}]^T \mathbf{e}^{(j)} \otimes [\mathbf{v}^{(i)}]^T \mathbf{v}^{(j)} \\
&= \delta_{ij}
\end{aligned} \tag{7}$$

and

$$\begin{aligned}
[\mathbf{u}^{(i)}]^T \mathbf{u}^{(j)} &= (\mathbf{e}^{(i)} \otimes \mathbf{u}^{(i)})^T (\mathbf{e}^{(j)} \otimes \mathbf{u}^{(j)}) \\
&= ([\mathbf{e}^{(i)}]^T \otimes [\mathbf{u}^{(i)}]^T) (\mathbf{e}^{(j)} \otimes \mathbf{u}^{(j)}) \\
&= [\mathbf{e}^{(i)}]^T \mathbf{e}^{(j)} \otimes [\mathbf{u}^{(i)}]^T \mathbf{u}^{(j)} \\
&= \delta_{ij}.
\end{aligned} \tag{8}$$

These results use that the Kronecker-product identity $(a \otimes b)(c \otimes d) = ac \otimes bd$ (assuming the dimensions appropriately match).

Provided that each $\mathbf{P}^{(i)}$ is nonnegative and irreducible, the dominant eigenvalue $\mu_1^{(i)} = 1$ of each $\mathbf{P}^{(i)}$ has geometric and algebraic multiplicity equal to 1. Thus the eigenvalue $\lambda_1 = 1$ of $\mathbb{P}(0)$ has geometric and algebraic multiplicity equal to I . The sets of eigenvectors $\{\mathbf{v}^{(i)}\}$ and $\{\mathbf{u}^{(i)}\}$ are eigenbases for the left and right eigenspaces for $\lambda_1 = 1$.

Next, we present our main analytical result for when there is a separation of time scales and transitions are far more likely to utilize an intralayer Markov chain versus an interlayer one.

Theorem II.3 Let $\mathbb{P}(\omega)$ be a supracentrality matrix of a multiplex Markov chain and assume each intralayer transition matrix $\mathbf{P}^{(i)}$ is nonnegative, irreducible, and has a dominant eigenvalue such that $\mu_1^{(i)} = 1$. We define $\mathbf{v}(0^+) = \lim_{\omega \rightarrow 0^+} \mathbf{v}(\omega)$ as the limiting left eigenvector of $\mathbb{P}(\omega)$. Then

$$\mathbf{v}(0^+) = \sum_{i=1}^I \tilde{\alpha}_i \mathbf{v}^{(i)}, \tag{9}$$

where the vector $\tilde{\alpha} = [\alpha_1, \dots, \alpha_I]^T$ has positive entries that satisfy $\sum_{i=1}^I \tilde{\alpha}_i = 1$ and is a unique solution to

$$\tilde{\alpha}^T \tilde{\mathbf{X}} = \tilde{\alpha}^T. \tag{10}$$

with

$$\tilde{X}_{ij} = \sum_{n=1}^N \tilde{P}_{ij}^{(n)} v_n^{(i)}. \tag{11}$$

Remark II.4 Since each $\tilde{\mathbf{P}}^{(n)}$ is row stochastic, matrix $\tilde{\mathbf{X}}$ is also row stochastic:

$$\begin{aligned}
\sum_j \tilde{X}_{ij} &= \sum_{n=1}^N \sum_j \tilde{P}_{ij}^{(n)} v_n^{(i)} \\
&= \sum_{n=1}^N v_n^{(i)} \\
&= 1.
\end{aligned} \tag{12}$$

It follows that $[1, \dots, 1]^T$ is a right eigenvector of $\tilde{\mathbf{X}}$ for an eigenvalue equal to 1. Therefore $\tilde{\mathbf{X}}$ is an “effective” interlayer transition matrix that represents a type of weighted aggregation of the interlayer Markov chains $\{\tilde{\mathbf{P}}^{(n)}\}$.

Remark II.5 When the intralayer Markov chains are uniformly coupled, i.e., $\tilde{\mathbf{P}}^{(n)} = \tilde{\mathbf{P}}$ for each node n , it then follows that $\tilde{\mathbf{X}} = \tilde{\mathbf{P}}$ and $\tilde{\alpha} = \tilde{\mathbf{v}}$, which is the left dominant eigenvector of $\tilde{\mathbf{P}}$.

Remark II.6 When the intralayer Markov chains have doubly stochastic transition matrices, i.e., $\sum_n P_{nm}^{(i)} = \sum_m P_{nm}^{(i)} = 1$ for each node i , then $v_n^{(i)} = 1/N$ for each i and $\tilde{\mathbf{X}}$ is the mean intralayer transition matrix.

Proof. Theorem II.1 proved that λ_1 has a P -dimensional left dominant eigenspace that are spanned by the left eigenvectors $\mathbf{v}^{(i)}$. The continuity of eigenvector spaces [11] ensures that $\mathbf{v}(0^+)$ converges to lie within this subspace, which implies Eq. (9). We now prove that the constants $\tilde{\alpha}_i$ satisfy Eqs. (10)-(11).

We Taylor expand $\mathbf{v}(\omega)$ for small ω as

$$\mathbf{v}(\omega) = \sum_{k=0}^K \omega^k \mathbf{v}_k + \mathcal{O}(\omega^{K+1}). \quad (13)$$

Successive terms in this expansion represent higher-order derivatives of $\mathbf{v}(\omega)$ with respect to ω , and we assume that $\mathbf{v}(\omega)$ has the appropriate smoothness [i.e., $\mathbf{v}(\omega) \in C^{(k)}(0, 1)$]. The $\omega \rightarrow 0^+$ limit of $\mathbf{v}(\omega)$ then becomes $\mathbf{v}_0 = \mathbf{v}(0^+)$. Focusing on the first-order approximation, we insert $\mathbf{v}(\omega) \approx \mathbf{v}_0 + \omega \mathbf{v}_1$ into the eigenvalue equation

$$\mathbf{v}(\omega) = \mathbb{P}(\omega)^T \mathbf{v}(\omega) \quad (14)$$

to obtain

$$\begin{aligned} \mathbf{v}_0 + \omega \mathbf{v}_1 &= (1 - \omega) \mathbb{P}(0)^T [\mathbf{v}_0 + \omega \mathbf{v}_1] + \omega \sum_n \left[(\tilde{\mathbf{P}}^{(n)} \otimes \mathbf{E}^{(n)})^T [\mathbf{v}_0 + \omega \mathbf{v}_1] \right] \\ &= \mathbb{P}(0)^T \mathbf{v}_0 + \omega \mathbb{P}(0)^T \mathbf{v}_1 - \omega \mathbb{P}(0)^T \mathbf{v}_0 - \omega^2 \mathbb{P}(0)^T \mathbf{v}_1 + \omega \sum_n \left[(\tilde{\mathbf{P}}^{(n)} \otimes \mathbf{E}^{(n)})^T \mathbf{v}_0 + \omega^2 \sum_n \left[(\tilde{\mathbf{P}}^{(n)} \otimes \mathbf{E}^{(n)})^T \mathbf{v}_1 \right] \right] \end{aligned} \quad (15)$$

The second-order terms will be negligible as $\omega \rightarrow 0$, and so we separately collect the zeroth-order and first-order terms in ω to obtain two consistency equations:

$$\mathbf{v}_0 = \mathbb{P}(0)^T \mathbf{v}_0 \quad (16)$$

and

$$\mathbf{v}_1 = \mathbb{P}(0)^T \mathbf{v}_1 - \mathbb{P}(0)^T \mathbf{v}_0 + \sum_n \left[(\tilde{\mathbf{P}}^{(n)} \otimes \mathbf{E}^{(n)})^T \mathbf{v}_0 \right]. \quad (17)$$

The consistency equation arising for the zeroth-order terms is exactly the eigenvalue equation with $\omega = 0$, as expected. It implies a solution of the form given by Eq. (9).

To proceed, we left multiply the consistency equation arising from the first-order terms by $\mathbf{u}^{(i)}$, yielding

$$[\mathbf{u}^{(i)}]^T \mathbf{v}_1 = [\mathbf{u}^{(i)}]^T \mathbb{P}(0)^T \mathbf{v}_1 - [\mathbf{u}^{(i)}]^T \mathbb{P}(0)^T \mathbf{v}_0 + \sum_n [\mathbf{u}^{(i)}]^T (\tilde{\mathbf{P}}^{(n)} \otimes \mathbf{E}^{(n)})^T \mathbf{v}_0. \quad (18)$$

However, $[\mathbf{u}^{(i)}]^T \mathbb{P}(0)^T = [\mathbf{u}^{(i)}]^T$ and the term on the left-hand side is canceled by the first term on the right-hand side, which yields

$$[\mathbf{u}^{(i)}]^T \mathbf{v}_0 = \sum_n \mathbf{u}^{(i)} (\tilde{\mathbf{P}}^{(n)} \otimes \mathbf{E}^{(n)})^T \mathbf{v}_0. \quad (19)$$

To simplify the left-hand side of Eq. (19), we use

$$\begin{aligned} [\mathbf{u}^{(i)}]^T &= [\mathbf{e}^{(i)} \otimes \mathbf{u}^{(i)}]^T \\ &= [\mathbf{e}^{(i)}]^T \otimes [\mathbf{u}^{(i)}]^T \end{aligned} \quad (20)$$

and $\mathbf{v}_0 = \sum_j \tilde{\alpha}_j (\mathbf{e}^{(j)} \otimes \mathbf{v}^{(j)})$ to obtain

$$\begin{aligned}
[\mathbf{u}^{(i)}]^T \mathbf{v}_0 &= \sum_j \tilde{\alpha}_j ([\mathbf{e}^{(i)}]^T \otimes [\mathbf{u}^{(i)}]^T) (\mathbf{e}^{(i)} \otimes \mathbf{v}^{(j)}) \\
&= \sum_j \tilde{\alpha}_j ([\mathbf{e}^{(i)}]^T \mathbf{e}^{(j)}) \otimes ([\mathbf{u}^{(i)}]^T \mathbf{v}^{(j)}) \\
&= \sum_j \tilde{\alpha}_j \delta_{ij} ([\mathbf{u}^{(i)}]^T \mathbf{v}^{(j)}) \\
&= \tilde{\alpha}_i ([\mathbf{u}^{(i)}]^T \mathbf{v}^{(i)}) \\
&= \tilde{\alpha}_i.
\end{aligned} \tag{21}$$

(Recall that $u_n^{(i)} = 1$ for each n and $\sum_n v_n^{(i)} = 1$.) Next we simplify the right-hand side of Eq. (19),

$$\begin{aligned}
\sum_n [\mathbf{u}^{(i)}]^T ([\tilde{\mathbf{P}}^{(n)}]^T \otimes [\mathbf{E}^{(n)}]^T) \mathbf{v}_0 &= \sum_n [\mathbf{u}^{(i)}]^T ([\tilde{\mathbf{P}}^{(n)}]^T \otimes [\mathbf{E}^{(n)}]^T) \sum_j \tilde{\alpha}_j \mathbf{v}^{(j)} \\
&= \sum_j \tilde{\alpha}_j \sum_n \left([\mathbf{e}^{(i)}]^T \otimes [\mathbf{u}^{(i)}]^T \right) \left([\tilde{\mathbf{P}}^{(n)}]^T \otimes [\mathbf{E}^{(n)}]^T \right) \left(\mathbf{e}^{(j)} \otimes \mathbf{v}^{(j)} \right) \\
&= \sum_j \tilde{\alpha}_j \sum_n \left([\mathbf{e}^{(i)}]^T [\tilde{\mathbf{P}}^{(n)}]^T \otimes [\mathbf{u}^{(i)}]^T [\mathbf{E}^{(n)}]^T \right) \left(\mathbf{e}^{(j)} \otimes \mathbf{v}^{(j)} \right) \\
&= \sum_j \tilde{\alpha}_j \sum_n \left([\mathbf{e}^{(i)}]^T [\tilde{\mathbf{P}}^{(n)}]^T \mathbf{e}^{(j)} \right) \otimes \left([\mathbf{u}^{(i)}]^T [\mathbf{E}^{(n)}]^T \mathbf{v}^{(j)} \right) \\
&= \sum_j \tilde{\alpha}_j \sum_n \left[\tilde{\mathbf{P}}^{(n)} \right]_{ij}^T u_n^{(i)} v_n^{(j)} \\
&= \sum_j \tilde{\alpha}_j \sum_n \tilde{P}_{ji}^{(n)} v_n^{(j)} \\
&= \sum_j \tilde{\alpha}_j X_{ji}.
\end{aligned} \tag{22}$$

Finally, we set Eq. (21) equal to Eq. (22) to obtain

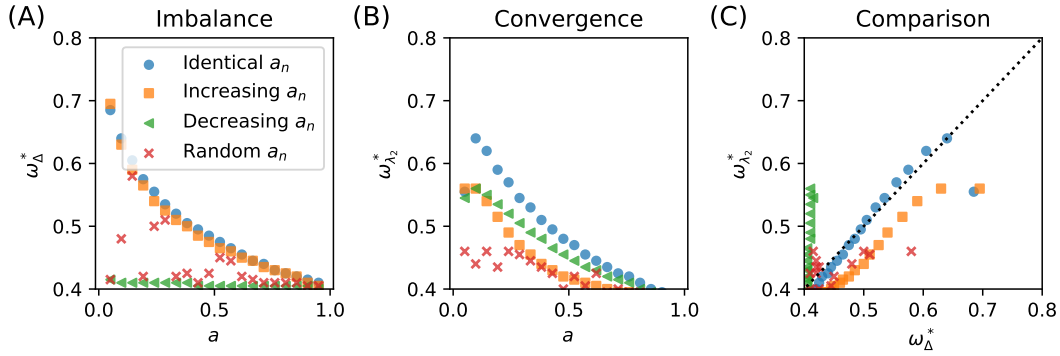
$$\tilde{\alpha}^T \tilde{\mathbf{X}} = \tilde{\alpha}^T. \tag{23}$$

III. EXTENDED STUDY OF OPTIMAL MULTIPLEX IMBALANCE

In Fig. 3 of the main text, it appears that there is a relationship between the value of ω at which the total multiplex imbalance $\|\Delta\|_F$ is optimized [which we denote $\omega_\Delta^* = \operatorname{argmax}_\omega \|\Delta\|_F \in (0, 1)$] and the value at which the convergence rate $\lambda_2(\omega)$ is optimized [which we denote $\omega_{\lambda_2}^* = \operatorname{argmax}_\omega \lambda_2(\omega)$]. To further explore the relationship between optimums $\omega_{\lambda_2}^*$ and ω_Δ^* , we repeated this experiment with many values of $a \in (0, 1)$. Recall that a tunes the heterogeneity of node-specific interlayer Markov chains, which have transition matrices $\tilde{\mathbf{P}}^{(n)} = \begin{bmatrix} (1-a_n) & a_n \\ a_n & (1-a_n) \end{bmatrix}$. Here the values a_n tune the probability of switching layers at each node n , and we considered four strategies for choosing a_n :

- (i) Identical a_n : we define $a_n = a$ for each n ;
- (ii) Increasing a_n : we define $a_n = a + (n-1)\delta a$ for $n \in \{1, \dots, N\}$ with $\delta a = (1-a)/(N-1)$;
- (iii) Decreasing a_n : we let $a_n = 1 - (n-1)\delta a$;
- (iv) Random a_n : we sample a_n uniformly at random from $[a, 1]$.

In Supplementary Fig. 2(A) and (B), we plot ω_Δ^* and $\omega_{\lambda_2}^*$, respectively, as a function of a . In each panel, we show results for the four strategies for creating interlayer Markov chains. Observe that in the limit $a \rightarrow 1$, all of the optimums occur at approximately the same coupling strength $\omega_{\lambda_2}^* \approx \omega_\Delta^* \approx 0.4$, which is expected since all four strategies yield uniform coupling: $\tilde{\mathbf{P}}^{(n)} \rightarrow \tilde{\mathbf{P}} = \begin{bmatrix} 0 & 1 \\ 1 & 0 \end{bmatrix}$. As one decreases a , the optimums shift to larger values of ω for all strategies except for the strategy with decreasing a_n . This response is largest for the strategies with identical a_n and increasing a_n , and it is less clear for the strategy with random a_n (in which case, the dependence of ω_Δ^* on a is more random).

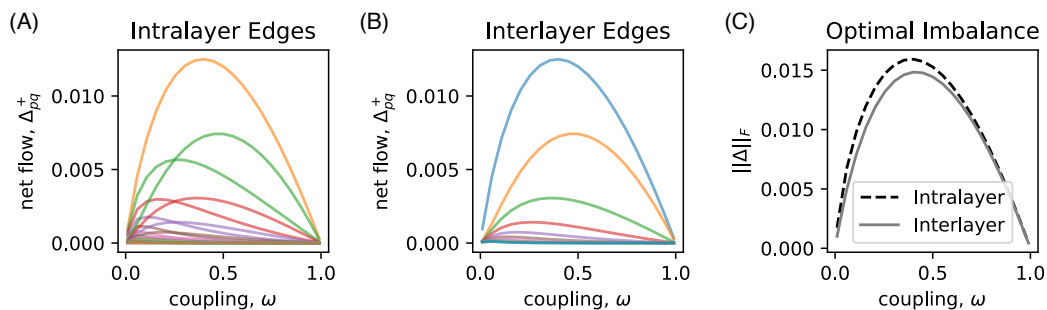


Supplementary Figure 2. **Relationship between optimality for multiplex imbalance and optimality for convergence rate.** For the experiment shown in Fig. 3 of the main text, we compare $\omega_{\Delta}^* = \operatorname{argmax}_{\omega} \|\Delta\|_F$ to $\omega_{\lambda_2}^* = \operatorname{argmax}_{\omega} \lambda_2(\omega)$. We show results for heterogeneous interlayer Markov chains in which the probability to move to a different layer at each node n is tuned by a_n , and we study four strategies for selecting a_n , each of which depends on a parameter a

In Supplementary Fig. 2(C), we compare $\omega_{\lambda_2}^*$ and ω_{Δ}^* across these values of a . Note for the strategy of identical a_n , that the two the optimums occur at nearly the same value of ω for any $a \in (0, 1)$ —that is, the blue squares lie along the diagonal. The dependence of $\omega_{\lambda_2}^*$ and ω_{Δ}^* on a is also strongly correlated for the strategy of increasing a_n ; however ω_{Δ}^* is always slightly larger than $\omega_{\lambda_2}^*$ and the relationship appears to be nonlinear for small a . The relation between $\omega_{\lambda_2}^*$ and ω_{Δ}^* appears to be random for the random strategy. Interestingly, for the strategy of decreasing a_n , $\omega_{\lambda_2}^*$ clearly increases with decreasing a , however ω_{Δ}^* appears to not depend on ω .

To gain intuitive insight, recall from Fig. 1(B) in the main text that the imbalance Δ_{pq} is largest for the edge connecting node 1 in layer 2 to node 1 in layer 1. That imbalance requires a net flow from node-layer pair $(1, 2)$ to $(1, 1)$, and this net flow monotonically increases with a_1 (i.e., since a_1 tunes the transition rate between layers). Therefore, we expect the multiplex imbalance to be most sensitive to a when a_1 changes with a . Parameter a_1 is most sensitive to a for the strategies of identical a_n and increasing a_n (i.e., $a_1 = a$ in these cases), it randomly depends on a for the strategy of random a_n (although it increases in expectation since $\mathbb{E}[a_n] = (1 + a)/2$), and it does not vary with a for the strategy of decreasing a_n (i.e., $a_1 = 1$). Therefore, our observed sensitivity with a for the different strategies is as one might expect based on our understanding for how degree-imbalance affect multiplex flow imbalances.

Next, we next study how each Δ_{pq} obtains an optimum at some value ω . In Supplementary Fig. 3, we plot each Δ_{pq} versus ω , and we separately plot the values for (A) intralayer edges [i.e., edges between node-layer pairs (n_p, i_p) and (n_q, i_q) with $i_q = i_p$] and (B) interlayer edges [i.e., edges between node-layer pairs (n_p, i_p) and (n_q, i_q) with $n_q = n_p$]. That is, we create the decomposition $\Delta = \Delta^{(intra)} + \Delta^{(inter)}$. Because the values Δ_{pq} come in pairs having opposite signs, i.e., since $\Delta_{pq} = -\Delta_{qp}$, we only plot positive Δ_{pq} . Observe in Fig. 3(A) and (B) that the Δ_{pq} value for some edges become much larger than those of others, and that the largest values obtain their maximum near $\omega \approx 0.45$. In contrast, the Δ_{qp} values that never become large tend to obtain their maximums at smaller $\omega \ll 0.45$. Interesting, we find for all edges that the sign of Δ_{pq} does not change. That is, the directions of net flows do not switch as ω varies, although it remains unclear if this is a general property of all multiplex networks.



Supplementary Figure 3. **Optimality of Δ_{pq} for each edge in a toy MMC.** We plot the positive Δ_{pq} values for each (A) intralayer and (B) interlayer edge for the MMC shown in Fig. 1 of the main text. In panel (C), we plot decompose $\Delta = \Delta^{(intra)} + \Delta^{(inter)}$ into two matrices, one corresponding to intralayer edges and the other corresponding to interlayer edges, and we plot their respective Frobenius norms vs ω .

In Supplementary Fig. 3(C), we plot $\|\Delta^{(intra)}\|_F$ and $\|\Delta^{(inter)}\|_F$, where $\Delta_{pq}^{(intra)} = \Delta_{pq}$ if the edge between p and q is an intralayer edge and $\Delta_{pq}^{(intra)} = 0$ otherwise. $\Delta_{pq}^{(inter)}$ is similarly defined. Note that $\|\Delta\|_F^2 = \|\Delta^{(intra)}\|_F^2 + \|\Delta^{(inter)}\|_F^2$. For this synthetic network (the same one from Fig. 1 in the main text), $\|\Delta^{(intra)}\|_F$ and $\|\Delta^{(inter)}\|_F$ are optimized at approximately the same spot: $\omega_\Delta^* \approx 0.45$.

IV. EXTENDED STUDY OF MMC MODEL FOR FREQUENCY-MULTIPLEXED FUNCTIONAL BRAIN NETWORKS

Here, we provide further results and insights on the optimality of multiplex imbalance for a MMC models of frequency-multiplexed functional brain networks using empirical data from [12]. The MMC has $N = 148$ nodes (brain regions) and $I = 7$ layers, which represent pairwise coherences of magnetoencephalography (MEG) signals at seven different frequency ranges: $\{[1, 4), [4, 8), [8, 10.5), [10.5, 13), [13, 20), [20, 30), [30, 45)\}$, which are measured in Hz. In this case, we couple each node across layers using node-specific interlayer Markov chains with transition matrices $\tilde{P}^{(n)}$ having entries

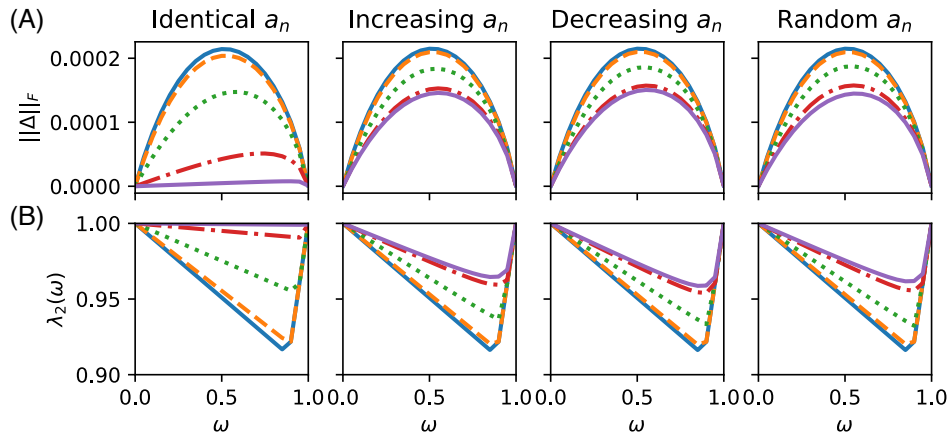
$$\tilde{P}_{ij}^{(n)} = \begin{cases} 1 - a_n, & i = j \\ a_n, & |i - j| = 1 \text{ and } i \in \{1, N\} \\ a_n/2, & |i - j| = 1 \text{ and } i \notin \{1, N\} \\ 0, & \text{otherwise} \end{cases}. \quad (24)$$

That is, we couple the Markov chain layer for each frequency band with those of the adjacent frequency bands with weight $a_n/2$ (with the exception of the the first and last layers, which are coupled by a_n).

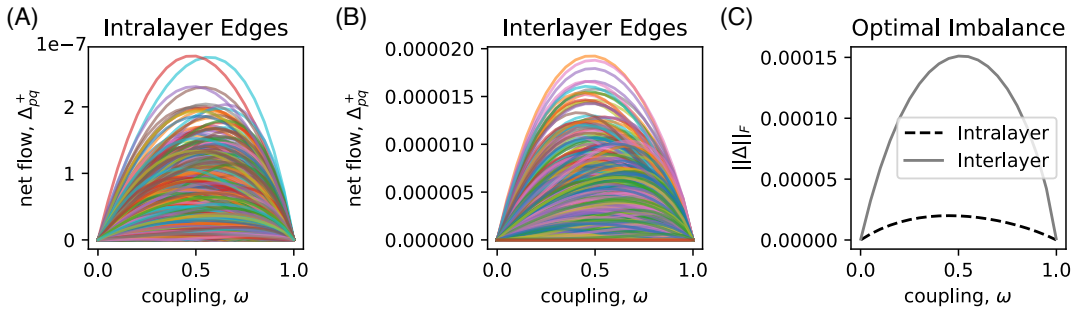
In Supplementary Fig. 4, we show a plot that is analogous to Fig. 3 in the main text, except we now show results for the brain dataset. The top panels depict the total multiplex imbalance $\|\Delta\|_F$, while the lower panels depict convergence rate $\lambda_2(\omega)$, both as a function of ω . Each column in Fig. 4 depicts curves for a different strategy for choosing the a_n values, and each depends on a parameter $a \in [0, 1]$ (see the description of Fig. 3 in the main to remind yourself of these four strategies). Observe that in this case, the locations ω_Δ^* and $\omega_{\lambda_2}^*$ of optima occur at very different values of ω , highlighting that optimality can more complicated when the number of Markov-chain layers increases (in this case there are $I = 7$ layers, whereas Fig. 3 in the main text shows results for $I = 2$ layers).

In Supplementary Fig. 5, we show a plot that is analogous to Fig. 3 on the previous page. We plot each Δ_{pq} versus ω for (A) intralayer edges and (B) interlayer edges, and in panel (C), we plot $\|\Delta^{(intra)}\|_F$ and $\|\Delta^{(inter)}\|_F$. Observe that in this case, the $\Delta_{pq}^{(intra)}$ values are on average about one-tenth as large as the $\Delta_{pq}^{(inter)}$ values.

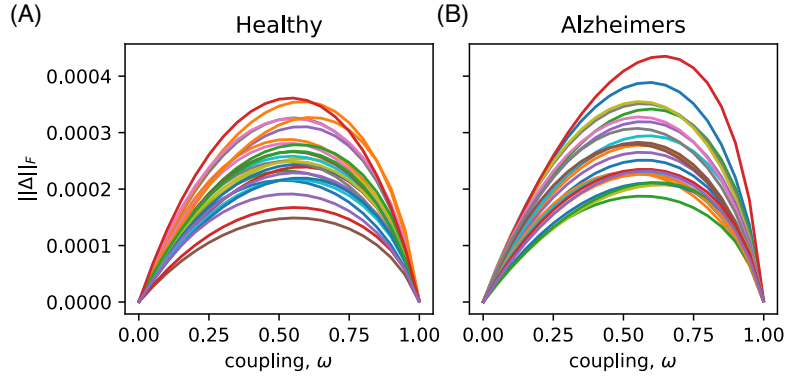
We next conducted a population-level study of multiplex imbalance and optimality for the 50 persons in the dataset from [12]: 25 healthy persons and 25 persons with Alzheimer's disease. In Supplementary Fig. 6, we plot $\|\Delta\|_F$ versus ω for (A) the healthy persons and (B) those with Alzheimer's disease. Observe that the $\|\Delta\|_F$ values are slightly larger for persons with the disease, and the value of ω at which the optimum occurs, ω_Δ^* , shifts slightly to the right. We find that the $\|\Delta\|_F$ values are larger



Supplementary Figure 4. **Optimality of multiplex imbalance and convergence rate for MMC model of a functional brain network** (A) Total multiplex imbalance $\|\Delta\|_F$ and (B) convergence rate $\lambda_2(\omega)$ versus ω for the same intralayer Markov chains as in Fig. 4 in the main text, except with node-specific interlayer Markov chains with transition matrices having entries: $\tilde{P}_{ij}^{(n)} = (1 - a_n)$ if $i = j$, $\tilde{P}_{ij}^{(n)} = a_n$ if $i = |j \pm 1|$, and $\tilde{P}_{ij}^{(n)} = 0$ otherwise. Each column depicts results for a different strategy for choosing the a_n values, and each depends on a parameter $a \in [0, 1]$.



Supplementary Figure 5. **Optimality of Δ_{pq} for each edge** We plot the positive Δ_{pq} values for each (A) intralayer and (B) interlayer edge in the MMC model of the brain. In panel (C), we plot decompose $\Delta = \Delta^{(intra)} + \Delta^{(inter)}$ into two matrices, one corresponding to intralayer edges and the other corresponding to interlayer edges, and we plot their respective Frobenius norms versus ω .



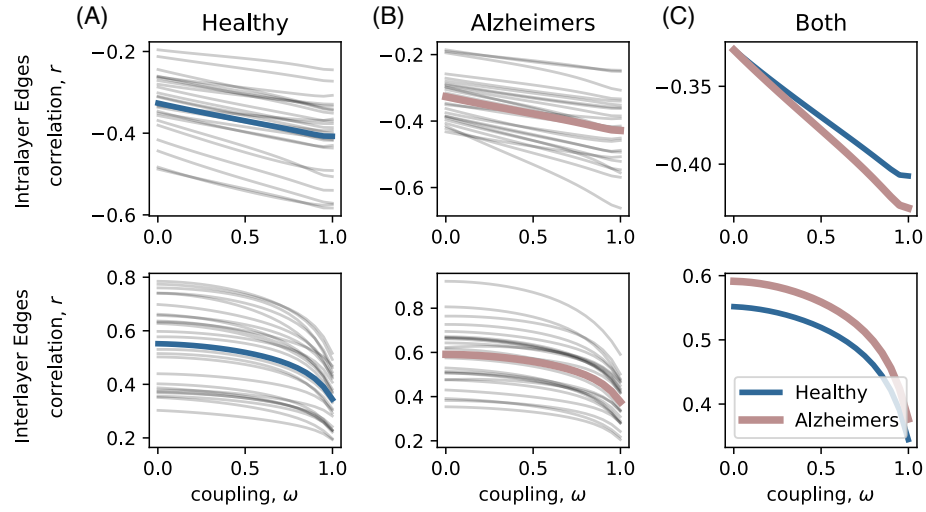
Supplementary Figure 6. **Optimal multiplex imbalance is different for persons with and without Alzheimers.** We plot $\|\Delta\|_F$ versus ω for 25 persons (A) without and (B) with Alzheimer's disease. Observe that the $\|\Delta\|_F$ values are slightly larger for persons with the disease, and the value of ω at which the optimum occurs, ω_{Δ}^* , shifts slightly to the right.

on average for persons with Alzheimer as compared to those without it. For example, when $\omega = 0.5$, $\|\Delta\|_F$ is 6.6% larger for persons with Alzheimers (0.000276 versus 0.000259). The average of $\omega_{\Delta}^* = \arg\max_{\omega} \|\Delta\|_F$ was also found to be 2.1% larger for persons with Alzheimers (0.570 versus 0.558).

We conclude this section by studying a mechanism that contributes to multiplex imbalance: large Δ_{pq} values arise for *inter-layer* edges such that the intralayer degree $d_n^{(i_p)}$ at node-layer pair (n, i_p) is much larger than that of (n, i_q) . This mechanism can be observed in Fig. 1(B) of the main text and was further studied in Fig. 3 in the main text.

In Supplementary Fig. 7, we plot the Pearson correlation coefficient between Δ_{pq} and $d_{n_p}^{(i_p)} - d_{n_q}^{(j_q)}$ versus ω for persons (left) with and (center) without Alzheimer's disease. Different curves correspond to different people and the thick colored curves indicate the mean curves. These means are also show in the right column to highlight the difference between persons with/without the disease. We separately computed these correlation coefficients for intralayer and interlayer edges, which we show in the upper and lower rows, respectively.

-
- [1] P. J. Mucha, T. Richardson, K. Macon, M. A. Porter, and J.-P. Onnela, *Science* **328**, 876 (2010).
 - [2] J.-C. Delvenne, S. N. Yaliraki, and M. Barahona, *Proceedings of the National Academy of Sciences* **107**, 12755 (2010).
 - [3] J. G. Kemeny and J. L. Snell, *Markov Chains* (Springer-Verlag, New York, 1976).
 - [4] S. Gómez, A. Díaz-Guilera, J. Gómez-Gardeñes, C. J. Pérez-Vicente, Y. Moreno, and A. Arenas, *Physical Review Letters* **110**, 028701 (2013).
 - [5] A. Solé-Ribalta, M. De Domenico, N. E. Kouvaris, A. Diaz-Guilera, S. Gomez, and A. Arenas, *Physical Review E* **88**, 032807 (2013).
 - [6] F. Radicchi and A. Arenas, *Nature Physics* **9**, 717 (2013).
 - [7] M. De Domenico, A. Solé-Ribalta, S. Gómez, and A. Arenas, *Proceedings of the National Academy of Sciences* **111**, 8351 (2014).
 - [8] A. Tejedor, A. Longjas, E. Fofoula-Georgiou, T. T. Georgiou, and Y. Moreno, *Physical Review X* **8**, 031071 (2018).
 - [9] G. Cencetti and F. Battiston, *New Journal of Physics* **21**, 035006 (2019).



Supplementary Figure 7. **Correlation between multiplex imbalance and imbalance of intralayer degrees.** We plot the Pearson correlation coefficient between Δ_{pq} and $d_{n_p}^{(i_p)} - d_{n_q}^{(j_q)}$ versus ω for persons (left) with and (center) without Alzheimer's disease. Different curves correspond to different people and the thick colored lines indicate the mean curves. These means are also show in the right column. The upper and lower rows correspond to intralayer and interlayer edges, respectively.

- [10] R. B. Bapat and T. E. S. Raghavan, *Nonnegative Matrices and Applications*, Vol. 64 (Cambridge University Press, Cambridge, UK, 1997).
 [11] T. Kato, *Perturbation Theory for Linear Operators*, Vol. 132 (Springer Science & Business Media, 2013).
 [12] J. Guillon, Y. Attal, O. Colliot, V. La Corte, B. Dubois, D. Schwartz, M. Chavez, and F. D. V. Fallani, *Scientific Reports* **7**, 1 (2017).